

Supplementary Information

Superior Fracture Resistance of Fiber Reinforced Polyampholyte Hydrogels Achieved by Extraordinarily Large Energy-dissipative Process Zones

Yiwan Huang,^a Daniel R. King,^{a,b} Wei Cui,^c Tao Lin Sun,^{a,b} Honglei Guo,^{a,b} Takayuki
Kurokawa,^{a,b} Hugh R. Brown,^e Chung-Yuen Hui,^f Jian Ping Gong*,^{a,b,d}

^a *Faculty of Advanced Life Science, Hokkaido University, Sapporo 001-0021, Japan*

^b *Soft Matter GI-CoRE, Hokkaido University, Japan*

^c *Graduate School of Life Science, Hokkaido University, Sapporo 001-0021, Japan*

^d *Institute for Chemical Reaction Design and Discovery (WPI-ICReDD), Hokkaido University,
N21W10, Kita-ku, Sapporo 001-0021, Japan*

^e *ARC Centre of Excellence for Electromaterials Science and Australian Institute for Innovative
Materials, University of Wollongong, Innovation Campus, Squires Way, North Wollongong,
NSW, 2522, Australia*

^f *Department of Mechanical and Aerospace Engineering, Field of Theoretical and Applied
Mechanics, Cornell University, Ithaca, NY 14853, USA*

* E-mail: gong@sci.hokudai.ac.jp

1. Supplementary Methods

Tensile Test: The tensile tests of the neat hydrogel samples were carried out by using a commercial tensile tester (Autograph AG-X, Shimadzu Co., Japan) equipped with a 100 N load cell at 100 mm min⁻¹ crosshead velocity in air. Before the tests, the samples were cut into a dumbbell shape standardized as JIS-K6251-7 (2 mm in inner width, 12 mm in gauge length) with a gel-cutting machine (Dumb Bell Co., Ltd.), as described in **Fig. S2a**. The tensile tests of the neat fabric and hydrogel composites were carried out by using the same tensile tester equipped with a 20 kN load cell at 100 mm min⁻¹ crosshead velocity in air. The neat fabric and composite samples were cut into a rectangular shape (20 mm $L \times$ 6.4 mm W) with a rotary cutter. The thickness of the neat hydrogel samples is 1 ~ 2 mm and the thickness of the other samples are given in **Fig. S9**. During the tests, a humidifier was used to supply a humid environment to minimize water evaporation of the gel samples. At least three tests were carried out for each sample, and the average value was calculated and the standard derivation was obtained as the error bar.

Tearing Test: The tearing energy of the samples was evaluated by a typical trouser tearing test.¹⁻⁵ In **Fig. 1a**, the geometry of trouser-shaped samples is sketched. A commercial tensile tester (Autograph AG-X, Shimadzu Co., Japan) equipped with a 1 kN load cell was used for the tearing test. The initial notch ($L_{\text{leg}} = 20$ mm) was placed nominally in the center of the sample with a rotary cutter. For neat gel samples, to prevent elongation of the legs of the samples during the tests, stiff and thin tapes were glued on the both sides of the samples prior to the tests, as described elsewhere in the literature.⁴ For large width composite samples, to prevent escape of the slippery samples from the clamps, each leg was sandwiched by two pieces of rectangular polymethyl methacrylate (PMMA) plate with skid-resistant wave-pattern before the tests, where the samples were adhered to the PMMA plates by using super glue. To guarantee initial pull-out or breaking of the transverse fiber bundles in the composite samples, the length required to break, L_{bulk} , of the samples was at least 5 mm larger than half of the

sample width W , i.e., $L_{\text{bulk}} > W/2 + 5$ mm. During the tests, one leg was clamped to the base, and the other leg was clamped to the crosshead, which was displaced at a constant velocity 50 mm min^{-1} to tear the sample and obtain the tearing force-displacement (F - Δ) curve. A humidifier was used to supply a humid environment to minimize water evaporation in both the neat hydrogel and composite samples during the tests. To evaluate the crack resistance capacity, the effective tearing energy, T , was calculated by integrating under F - Δ curve to determine the work required to break the samples, and divided by the fracture area, which is L_{bulk} multiplied by the thickness of the sample, t :

$$T = \frac{\int_0^{\Delta} F d\Delta}{t * L_{\text{bulk}}} \quad (\text{S1})$$

This method has been reported previously⁶ and was also described in detail in our previous studies.^{2,3} As revealed in **Fig. 2a**, **S6**, and **S8**, the fracture paths in our composite samples show curvature, we therefore use the real path length, L_{bulk}' (the green dotted lines in **Fig. 2a**, **S6**, and **S8**), instead of the nominal L_{bulk} for the estimation of tearing energy. Here the fracture path of each composite sample was determined approximately by the fractured hydrogel matrix boundary. Because the tearing force for the composite samples tested here is much larger compared to that of the neat gels shows in the same condition, the fabric thickness, t , was used to calculate the tearing energy of the composite samples. At least three tests were carried out for each sample, and the average value was calculated and the standard derivation was obtained as the error bar.

Scanning Electron Microscopy: The surface morphologies of the neat fabrics and the fractured composite samples were captured with a scanning electron microscope (SEM, JEOL JSM-6010LA, Tokyo, Japan). For the composite samples, after the tearing test, the samples were dried at $60 \text{ }^\circ\text{C}$ in an oven for two days. Before observation, the samples were gold-coated

in an ion-sputtering machine (E-1010, Hitachi, Tokyo, Japan). During the observation, the acceleration voltage varied from 10 to 20 kV.

2. Supplementary Figures

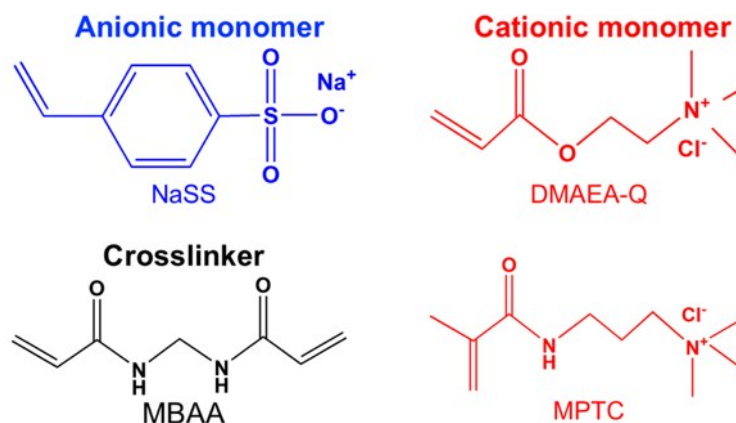


Fig. S1. Chemical structures of the monomers and crosslinker for preparation of polyampholyte (PA) hydrogels. NaSS: sodium *p*-styrenesulfonate; DMAEA-Q: dimethylaminoethylacrylate quaternized ammonium; MPTC: 3-(methacryloylamino)propyl-trimethylammonium chloride; MBAA: *N,N'*-methylene-bis-acrylamide.

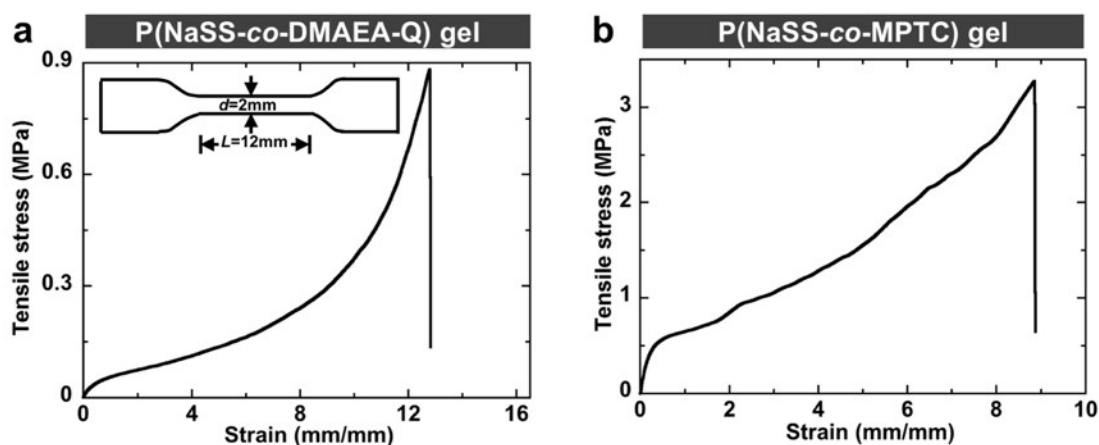


Fig. S2. Tensile behaviors of the two polyampholyte hydrogels, P(NaSS-*co*-DMAEA-Q) gel and P(NaSS-*co*-MPTC) gel used as soft matrices in this work. The geometry of dumbbell-shaped sample for the tensile tests is shown in the insert of the figure (a). Tensile velocity is 100 mm min⁻¹. The neat hydrogel samples were cut into a dumbbell shape

standardized as JIS-K6251-7 (2 mm in inner width, 12 mm in gauge length, and 1 ~ 2 mm in sample thickness) with a gel-cutting machine (Dumb Bell Co., Ltd.).

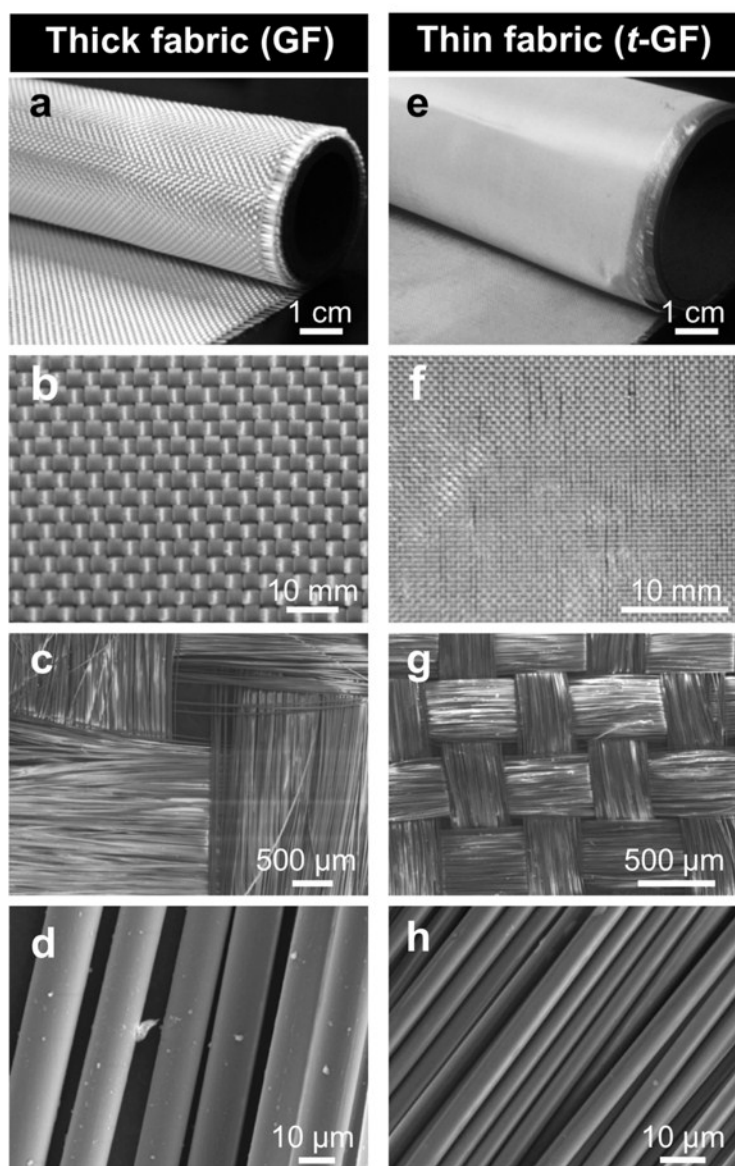


Fig. S3. Macro- and micrographs of two kinds of plain weave glass fabrics from E-glass used in this work. Macrographs of the commercially available glass fabrics (**a**, **e**) and the plain weave structures (**b**, **f**). SEM micrographs of a single weave of the fabrics (**c**, **g**) and individual glass fibers (**d**, **h**). Here thick and thin fabrics are denoted as GF and *t*-GF, respectively. The basic structures and mechanical parameters of the both fabrics are listed in **Table S2**.

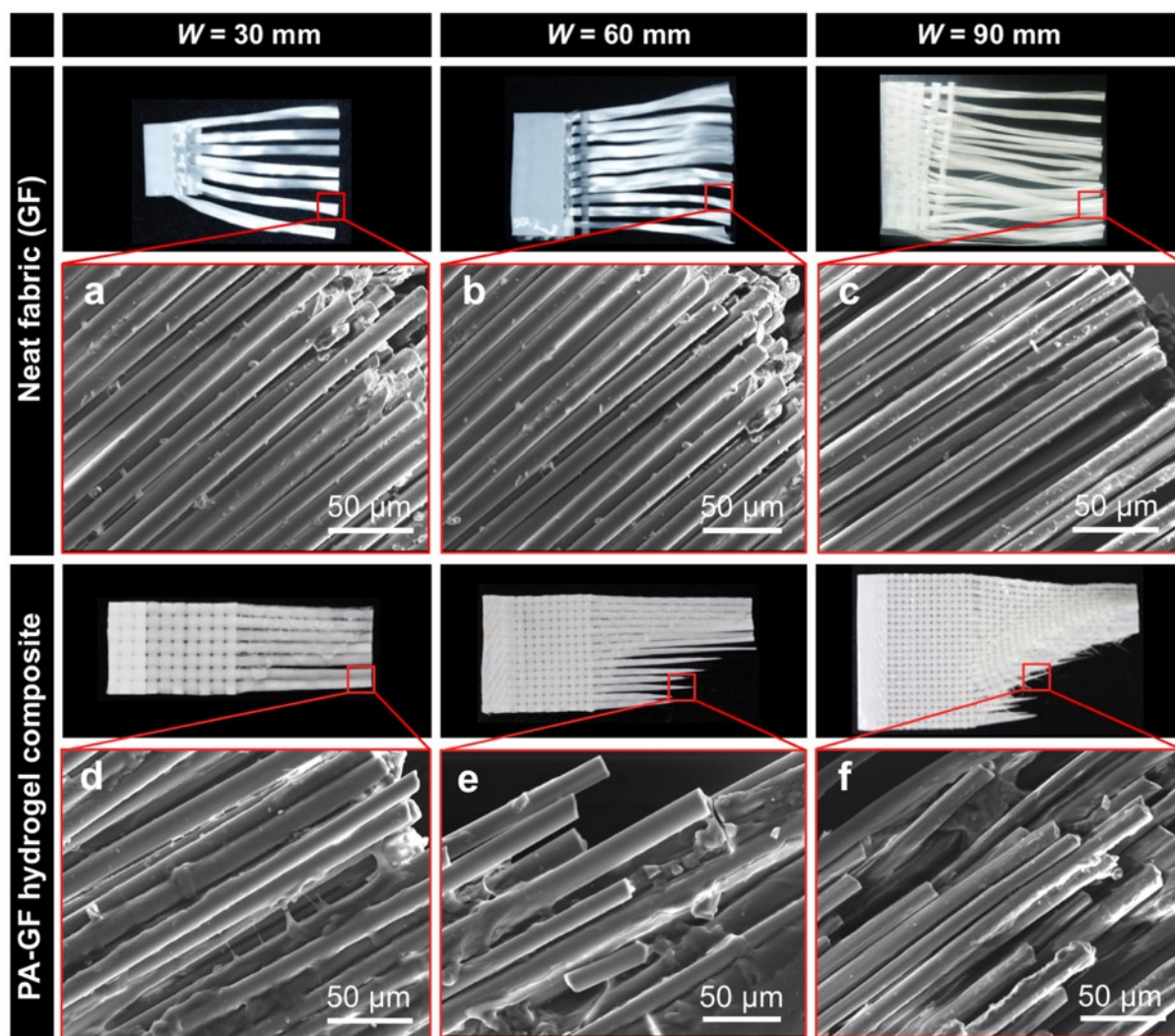


Fig. S4. Macro- and micrographs of fractured neat GF and PA-GF hydrogel composites with different sample widths, W . One leg of the fractured samples after the tearing tests was shown for the macroscopic images. P(NaSS-*co*-DMAEA-Q) gel was used as soft matrix in the composites.

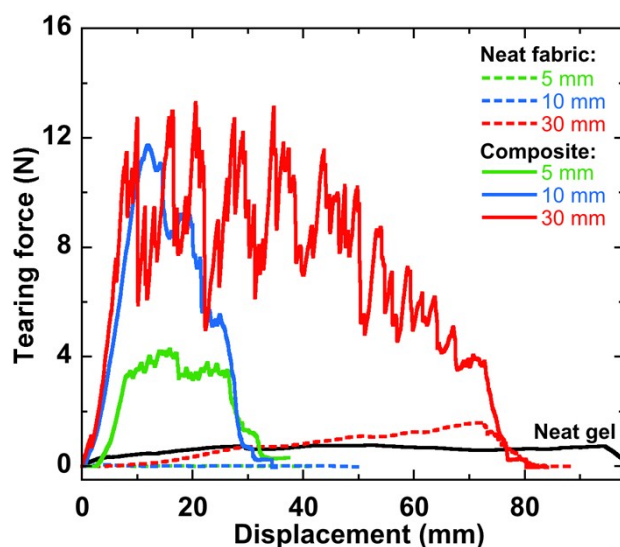


Fig. S5. Tearing force versus displacement curves for neat *t*-GF, neat PA gels, and PA-*t*-GF gel composites. Three sample widths (i.e., 5 mm, 10 mm, and 30 mm) for both the neat *t*-GF and composites are shown. The thicknesses for the *t*-GF, PA gel, and gel composites are 0.045 mm, 0.43 mm, and 0.49 mm, respectively. P(NaSS-*co*-DMAEA-Q) gel was used as soft matrix in the composites.

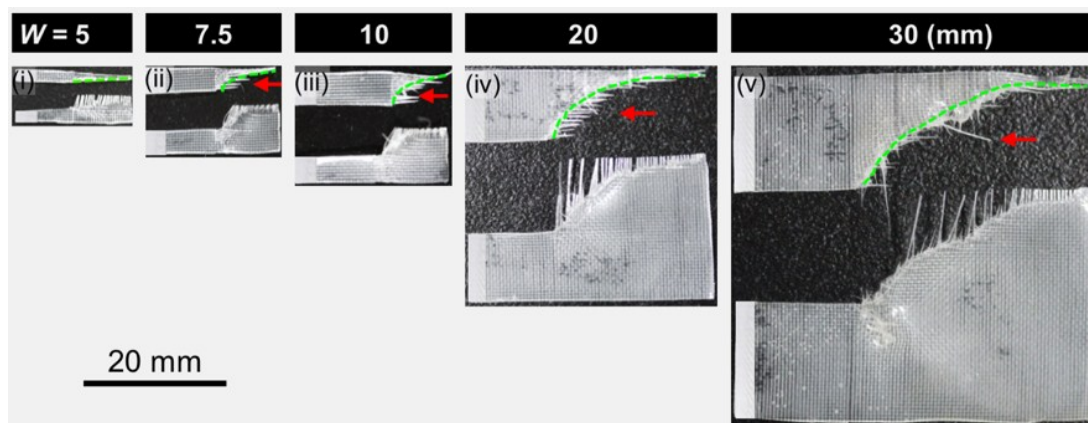


Fig. S6. Macrographs of the fractured PA-*t*-GF hydrogel composites with varied sample width, W . The different sample widths were also selected for demonstrating the three failure modes in the composites. The red arrows indicate the breaking of fiber bundles, and the green dashed lines represent the true fracture path length, L_{bulk} , used to calculate the tearing energy. Here the fracture path of each sample was determined approximately by the fractured hydrogel matrix boundary. P(NaSS-*co*-DMAEA-Q) gel was used as soft matrix in the composites.

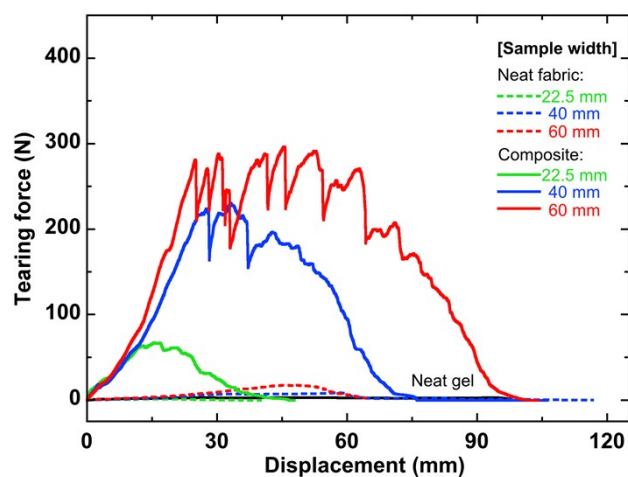


Fig. S7. Tearing force versus displacement curves for neat GF, neat PA gels, and PA- GF gel composites. Three sample widths (i.e., 22.5 mm, 40 mm, and 60 mm) for both the neat GF and composites are shown. Relatively thick glass fabric (GF) was used to fabricate the composites. P(NaSS-*co*-MPTC) gel was used as soft matrix in the composites.

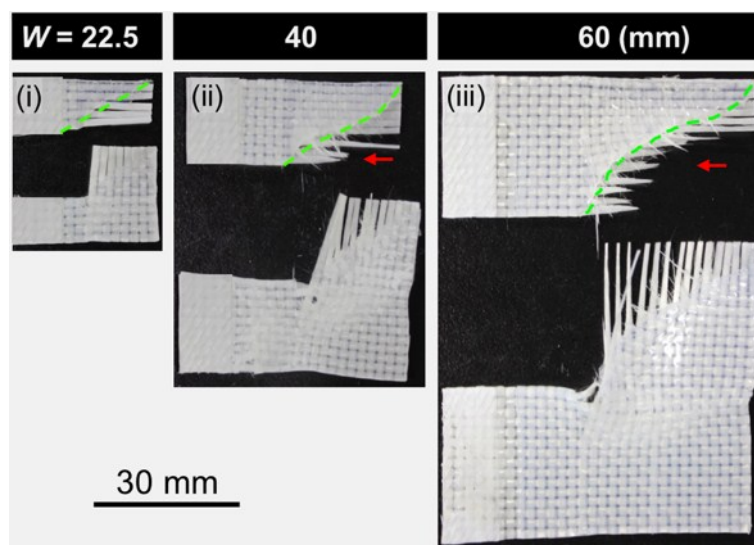


Fig. S8. Macrographs of the fractured PA-GF hydrogel composites with varied sample width, W . The three sample widths were chosen for demonstrating the different failure modes in the composites. The red arrows indicate the breaking of fiber bundles, and the green dashed lines represent the true fracture path length, L_{bulk} , used to calculate the tearing energy. Here the fracture path of each sample was determined approximately by the fractured hydrogel matrix boundary. P(NaSS-*co*-MPTC) gel was used as soft matrix in the composites.

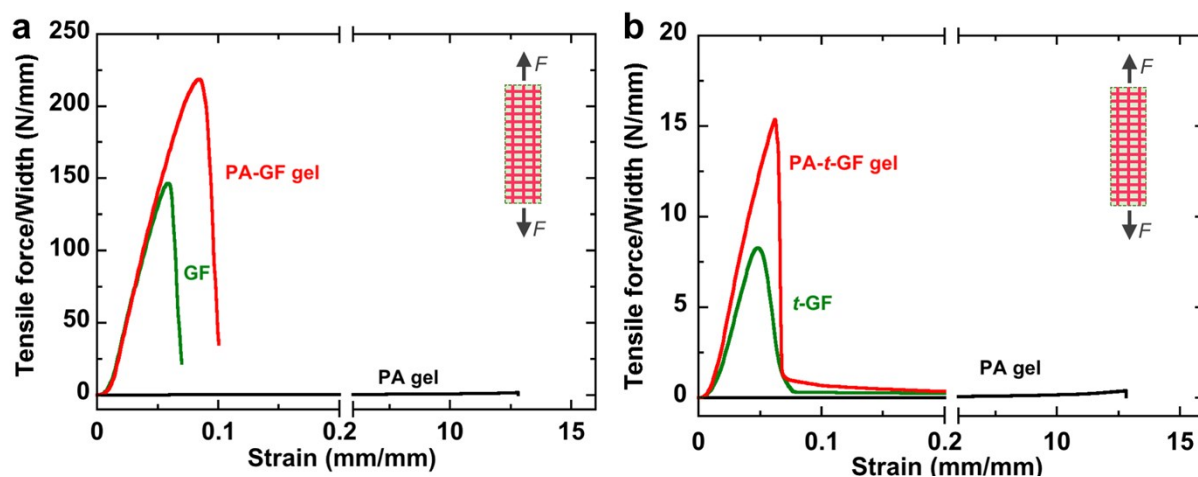


Fig. S9. Tensile behaviors of neat PA gel, neat GF and *t*-GF, and their composites. As shown in the inserted schematic illustration, the applied tensile force is parallel to the fiber alignment. Sample dimension (rectangular shape) detail: (a) neat GF: gauge length $L = 20$ mm, width $W = 6.4$ mm, thickness $t = 0.59$ mm; PA-GF composite: $L = 20$ mm, $W = 6.4$ mm, $t = 1.07$ mm; (b) neat *t*-GF: $L = 20$ mm, $W = 4$ mm, $t = 0.045$ mm; PA-*t*-GF composite: $L = 20$ mm, $W = 4$ mm, $t = 0.49$ mm. Sample dimension (dumbbell shape) detail: neat PA gel: $L = 12$ mm, $W = 2$ mm, $t = 1.73$ mm. The detailed tensile properties are shown in **Table S3**. P(NaSS-*co*-DMAEA-Q) gel was used as soft matrix in the composites.

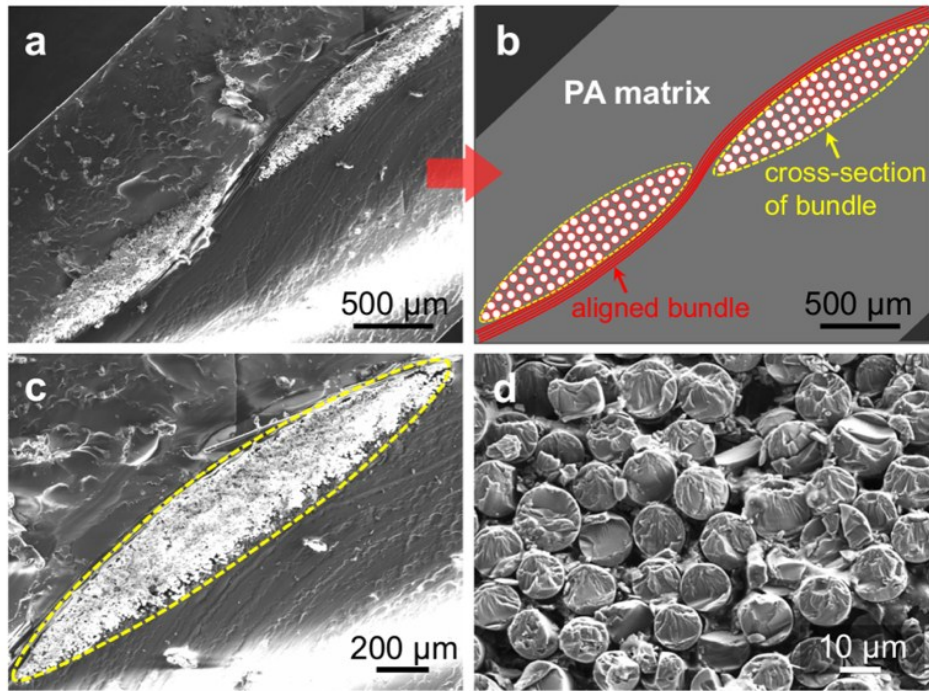


Fig. S10. SEM images for calculation of the cross-sectional perimeter of a single bundle in the PA-GF hydrogel composites. (a) The cross-sectional image of the composite shows the existence of the fabric in the composite, which is further illustrated in (b). (c) The magnified image of a bundle. The image (d) shows the dense packing of small fibers in the bundle. The cross-sectional perimeter of a bundle (S) measured from the images, $S = 4.3 \pm 0.2$ mm ($N > 5$).

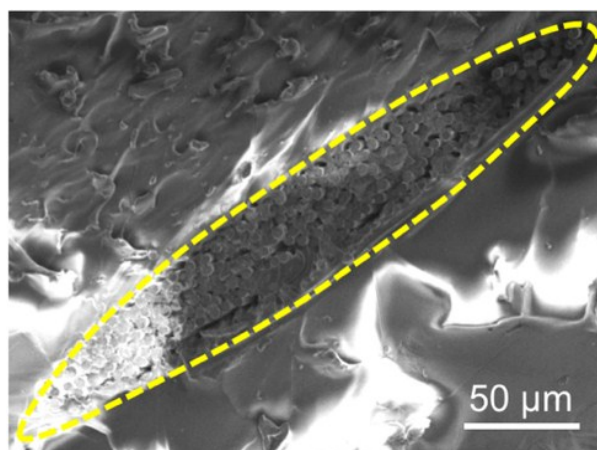


Fig. S11. SEM image for calculation of the cross-sectional area of a single bundle in the PA-*t*-GF hydrogel composite. The cross-sectional perimeter of the bundle (S) measured from the images, $S = 0.68 \pm 0.03$ mm ($N > 5$).

3. Supplementary Tables

Table S1. Mechanical parameters of the two kinds of polyampholyte hydrogels used in this work.

PA gels	Water content (wt%)	Young's modulus E (MPa)	Fracture strength σ_b (MPa)	Fracture strain ϵ_b (mm mm ⁻¹)	Work of extension at fracture W_{ext} (MJ m ⁻³)	Fracture energy G_c (kJ m ⁻²)
P(NaSS-co-DMAEA-Q)	48 ± 1	0.13 ± 0.02	0.95 ± 0.09	14 ± 1	3.9 ± 0.4	3.5 ± 0.2
P(NaSS-co-MPTC)	46 ± 1	2.8 ± 0.4	3.2 ± 0.4	8.1 ± 0.8	13 ± 2	5.7 ± 0.8

a) The errors ranges are standard deviations on at least three samples.

Table S2. Structural and mechanical parameters of the two kinds of plain weave glass fabrics used in this work. The SEM images of the glass fabrics are shown in Figure S3.

Fabrics	Fabric area density σ_a (g m ⁻²)	Fabric thickness t (mm)	Cross-sectional perimeter of fiber bundle S^a (mm)	Cross-sectional area of fiber bundle A (mm ²)	Single fiber radius r (μm)	Fiber bundle tensile fracture force F_f (N)
GF	590	0.59	4.3 ± 0.2	0.41 ± 0.04	7	375 ± 17
<i>t</i> -GF	47	0.045	0.68 ± 0.03	0.008 ± 0.001	2.5	3.6 ± 0.1

a) S was estimated from the corresponding composites. The errors ranges are standard deviations on at least three samples.

Table S3. Tensile properties of the neat glass fabrics and their composites with P(NaSS-co-DMAEA-Q) gel matrix.

Samples	Modulus $E^a)$ (MPa)	Fracture strength $\sigma_b^a)$ (MPa)	Fracture strain ε_b (mm mm ⁻¹)	Work of extension $W_{\text{ext}}^a)$ (MJ m ⁻³)
Neat GF	5487 ± 44	242 ± 11	0.072 ± 0.001	8.0 ± 0.5
Neat <i>t</i> -GF	5800 ± 140	188 ± 4	0.075 ± 0.026	7.0 ± 0.7
PA-GF Composite	5347 ± 100	324 ± 66	0.101 ± 0.004	18 ± 4
PA- <i>t</i> -GF Composite	7066 ± 520	321 ± 30	0.115 ± 0.039	15 ± 1

a) Because the fracture for the composite samples occurred at a very small strain, and the load supported by the soft gel at this strain was extremely low, the fracture strength of the composites, σ_b , was calculated from the maximum load divided by the cross-sectional area of neat fabric before loading (the width, W , multiplied by the fabric thickness, t) for both the neat fabric and composite. Modulus, E , was calculated from the slope of stress-strain curve within 20% strain. Work of extension at fracture, W_{ext} , was calculated from the strain energy divided by the cross-sectional area of the neat fabric for both the neat fabric and composite. The errors ranges are standard deviations on at least three samples.

4. Supplementary References

- 1 T. L. Sun, T. Kurokawa, S. Kuroda, A. Bin Ihsan, T. Akasaki, K. Sato, M. A. Haque, T. Nakajima and J. P. Gong, *Nat. Mater.*, 2013, **12**, 932–937.
- 2 D. R. King, T. L. Sun, Y. Huang, T. Kurokawa, T. Nonoyama, A. J. Crosby and J. P. Gong, *Mater. Horiz.*, 2015, **2**, 584–591.
- 3 Y. Huang, D. R. King, T. L. Sun, T. Nonoyama, T. Kurokawa, T. Nakajima and J. P. Gong, *Adv. Funct. Mater.*, 2017, **27**, 1605350.
- 4 J.-Y. Sun, X. Zhao, W. R. K. Illeperuma, O. Chaudhuri, K. H. Oh, D. J. Mooney, J. J. Vlassak and Z. Suo, *Nature*, 2012, **489**, 133–136.

- 5 R. S. Rivlin and A. G. Thomas, *J. Polym. Sci.* 1953, **10**, 291.
- 6 E. Triki, P. Dolez and T. Vu-Khanh, *Compos. Part B Eng.* 2011, **42**, 1851.